Smart Structures and Systems, *Vol. 28, No. 3 (2021) 407-423*
https://doi.org/10.12989/sss.2021.28.3.407

Model-free identification of multiple periodic excitations and detection of structural anomaly using noisy response measurements

Z.G. Ying [1,2a], Y.W. Wang [1b], Y.Q. Ni*[1] and C. Xu [1b]

[1] *Hong Kong Branch of National Rail Transit Electrification and Automation Engineering Technology Research Center, Department of Civil and Environmental Engineering, The Hong Kong Polytechnic University, Hung Hom, Kowloon, Hong Kong S.A.R.*
[2] *Department of Mechanics, School of Aeronautics and Astronautics, Zhejiang University, Hangzhou 310027, P.R. China*

(*Received December 7, 2020, Revised April 23, 2021, Accepted April 28, 2021*)

Abstract. Anomaly and damage detection is an important research topic in the field of structural health monitoring (SHM). It is in general difficult to establish a precise computational model and measure multiple dynamic loads for complex structures. Model-free identification methods using only response measurements are therefore highly desired. Based on second-order statistics blind separation (SOSBS), this study explores response-only blind excitation separation and structural feature extraction when the structure is subject to multiple periodic excitations. The proposed method proceeds with two steps: (i) a transformation to convert the measurement space to eigenspace with identity covariance matrix and compact the measurement dimension to independent source dimension; and (ii) joint diagonalization of covariances with various time shifts to determine the mixture features. Neither structural model nor measurement of excitations is required in this method, and the extracted mixture matrix representative of structural dynamic characteristics can be used for structural anomaly detection and damage diagnosis. Both numerical simulation of a 3-degree-of-freedom vibration system and experimental study of a 5-story physical structure are conducted to verify the proposed method.

Keywords: blind excitation separation; model-free and response-only approach; multiple periodic excitations; second-order statistics; structural anomaly detection

1. Introduction

Structural health monitoring (SHM) and damage diagnosis is an important research theme in the engineering community (Carden and Fanning 2004, Spencer *et al*. 2004, Ko and Ni 2005, Deraemaeker and Worden 2010, Brownjohn *et al*. 2011, Fan and Qiao 2011, Goyal and Pabla 2016, Seo *et al*. 2016, Li *et al*. 2016, Li and Ou 2016, Yang and Chen 2016, Moughty and Casas 2017). A common way of SHM is to make use of structural dynamic responses for identifying the change in modal properties and relating it to structural damage (Dessi and Camerlengo 2015, Ciambella *et al*. 2019, Ying *et al*. 2019). In general, high-order vibration modes are sensitive to damage but difficult to accurately identify. Singular value decomposetion and distance-based analysis of feature matrix elicited from frequency responses have been used for damage detection (Vanlanduit *et al*. 2005). Bayesian probabilistic inference and machine learning methods have been proposed for structural identification under noisy measurements (Sohn and Law 1997, Beck and Katafygiotis 1998, Vanik *et al*. 2000, Zhang *et al*. 2016, Prajapat and Ray-Chaudhuri 2018, Bull *et al*. 2019, Ghiasi *et al*. 2021). However, for complex large-scale structures, inaccurate computational models may result in unreliable feature identification, and the external loadings acting on such structures, which are in general of distributed type, are difficult to measure. Hence, model-free identification methods with use of only response measurements have been in the spotlight at present. Unawareness of both excitations and structural properties imposes a challenge to damage diagnosis since it makes the feature identification problem undetermined. A variety of system identification methods using only dynamic response measurements have been developed in the past two decades. The stochastic subspace method was proposed for modal parameter extraction with the use of structural responses and correlation functions (Overschee and Moor 1996, Peeters and De Roeck 2001, Weng *et al*. 2009, Giraldo *et al*. 2009, Wu *et al*. 2019). This method assumes that excitation is a white noise process and responses at different time instants are fully uncorrelated. Recently, signal processing techniques for blind source separation have been applied to modal extraction and damage identification. For example, independent component analysis was pursued for extraction of vibration modes and modal responses by using structural responses statistics (Hyvarinen and Oja 2000, Kerschen *et al*. 2007, Yang and Nagarajaiah 2014, Nagarajaiah and Yang 2015, Sadhu *et al*. 2017) and was applied to detect blade crack and bearing composite faults (He *et al*. 2018, Li *et al*. 2019). This method assumes that the number of extraction sources is known, and the sources are fully independent

*Corresponding author, Ph.D., Chair Professor,
E-mail: ceyqni@polyu.edu.hk
[a] Professor
[b] Ph.D.

ISSN: 1738-1584 (Print), 1738-1991 (Online)

non-Gaussian processes expressive by high-order statistics. As the relationship between an excitation and its response depicts the local dynamic characteristics of a structure, perceiving alteration in this relationship is a direct approach to structural anomaly identification and damage diagnosis. To achieve this, blind excitation separation is necessary in the situation of unknown excitations.

For a model-unaware structure subject to unknown excitations, model-free data-driven identification using only response measurements involves separating blind excitations and determining feature relationship between responses and excitations. In the signal processing community, a blind source separation method using signal second-order statistics has been developed to extract simultaneously the mixture and sources and it is suitable for periodic and Gaussian sources (Tong *et al*. 1990, Belouchrani *et al*. 1997, Belouchrani and Amin 1998, Yeredor 2000, Abed-Meraim *et al*. 2001, Parra and Sajda 2003, Bouguerriou *et al*. 2005). The second-order statistics blind separation (SOSBS) method has been applied to structural modal identification (McNeill and Zimmerman 2008, Antoni and Chauhan 2013, Sadhu and Narasimhan 2014, Musafere *et al*. 2016, Brewick and Smyth 2017, Rainieri *et al*. 2019). However, in free vibration of a damped structure, the structural and modal responses are non-stationary, and the number of modes is restricted in analysis. Furthermore, in randomly excizzted vibration, modal responses are not independent sources. Therefore, the capability of SOSBS for modal identification is limited. In reality, many structures are subject to combined periodic and random excitations. For example, moving loads in different velocities passing through a bridge are periodic excitations that generate responses in discrete harmonics domain. Periodic excitations are concomitant of machines due to eccentric rotation in multi-story factory buildings with elevated machines at various floors, where the multiple-frequency responses are a mixture of periodic sources. Also, stationary responses measured from a structure subject to multiple excitations can be viewed as algebraic mixture of periodic excitations contaminated with noise. In such situations, the SOSBS would be effective to blind excitation separation and structural feature extraction, but yet to be studied.

In this study, a novel data-driven approach which enables blind excitation separation and structural feature extraction for damage diagnosis is proposed. Making use of response measurements under periodic excitations contaminated with noise, the number of excitation sources is determined by the eigenvalues of the correlation matrix of the measured responses. After converting the measurement space to eigenspace with identity covariance matrix and compacting the measurement dimension into independent source dimension, joint diagonalization for covariances with various time shifts is achieved to elicit the mixture feature. A change in the elements of the mixture feature matrix can alarm the occurrence of structural anomaly or damage.

The contribution of this study is twofold: (i) SOSBS is firstly attempted to separate the multiple periodic excitations acting on a multi-degree-of-freedom (multi-DOF) system without the help of a computational model; (ii) an anomaly index is formulated using the extracted mixture features for structural damage diagnosis. The rest of the paper is organized as follows. Section 2 introduces the SOSBS. Section 3 presents the SOSBS-based method for excitation separation and structural anomaly detection. In Section 4, numerical simulation of a 3-DOF vibration system is pursued to examine the robustness in extracting mixture features under different excitation frequencies, measurement noise and system damping, and the ability to separate multiple periodic excitations when being mixed with relatively light and band-limited random excitation. In Section 5, a 5-story frame structure is tested to examine the sensitivity of the extracted mixture features to structural damage by comparing it with the sensitivity of modal frequencies, and the variation of the extracted mixture features in regard to different damage severities. Conclusions are drawn in Section 6.

2. Second-order statistics blind separation (SOSBS)

In a blind source separation problem, multiple source signals and their mixture are unknown, while only multiple output measurements are available. The problem is stated as (Belouchrani *et al*. 1997)

$$\mathbf{Y}(t) = \mathbf{H}\mathbf{F}(t) + \mathbf{W}(t) \tag{1}$$

where $\mathbf{Y}$ is the k-dimensional measurement vector, $\mathbf{F}$ the n-dimensional source vector, $\mathbf{H}$ the $k \times n$-dimensional mixture matrix, and $\mathbf{W}$ the k-dimensional noise vector with zero mean. The system is unknown and the mixture (matrix) synthetically represents the system dynamic characteristics between sources (periodic excitations or their variants) and output measurements (stationary responses). The objective is to obtain the mixture $\mathbf{H}$ and sources $\mathbf{F}$ based on the measurements $\mathbf{Y}$. At an instant, the sources $\mathbf{F}$ and mixture $\mathbf{H}$ cannot be separated and determined by only the instantaneous measurements $\mathbf{Y}$. However, with the measurements $\mathbf{Y}$ within a certain time interval, the sources $\mathbf{F}$ and mixture $\mathbf{H}$ can be estimated and separated by using their statistics. It is assumed in this study that $k \geq n$, the mixture $\mathbf{H}$ is constant, and the sources $\mathbf{F}$ are independent of each other. In a certain time interval, the sources $\mathbf{F}$ are considered as stationary processes and thus the measurements $\mathbf{Y}$ are stationary as well. The sources $\mathbf{F}$ are further regarded as ergodic processes such that the event statistics can be estimated by using time statistics.

The execution of SOSBS comprises two main steps. First, a transformation is conducted to convert the measurement space to eigenspace with identity covariance matrix and compact the measurement dimension into independent source dimension. That is

$$\mathbf{Z}(t) = \mathbf{T}\mathbf{Y}(t) = \mathbf{T}\mathbf{H}\mathbf{F}(t) + \mathbf{T}\mathbf{W}(t) \tag{2}$$

where $\mathbf{T}$ is the $n \times k$-dimensional transformation matrix, and $\mathbf{Z}$ is the n-dimensional transformed vector. With Eq.

(2), the covariance operation without time shift yields

$$\mathbf{T}[\mathbf{C_Y}(0) - \mathbf{C_W}(0)]\mathbf{T}^{\mathrm{T}} = \mathbf{T}\mathbf{H}\mathbf{C_F}(0)(\mathbf{T}\mathbf{H})^{\mathrm{T}} \tag{3}$$

where $\mathbf{C_Y}$, $\mathbf{C_F}$, $\mathbf{C_W}$ are the covariance matrices of the measurements $\mathbf{Y}$, sources $\mathbf{F}$ and noises $\mathbf{W}$, respectively. The transformation $\mathbf{T}$ makes the right-hand side of Eq. (3) to be an identity matrix, that is

$$\mathbf{T}[\mathbf{C_Y}(0) - \mathbf{C_W}(0)]\mathbf{T}^{\mathrm{T}} = \mathbf{I} \tag{4}$$

By imposing singular value decomposition for the covariance matrix on the left-hand side of Eq. (4), the following relation is obtained

$$\mathbf{T}\mathbf{U}\mathbf{\Lambda}^{1/2} = \mathbf{I} \tag{5}$$

and thus the transformation $\mathbf{T}$ becomes

$$\mathbf{T} = \mathbf{\Lambda}^{-1/2}\mathbf{U}^{\mathrm{T}} \tag{6}$$

where the superscript T denotes the generalized transpose, $\mathbf{U}$ is the unitary matrix, and $\mathbf{\Lambda}$ is the diagonal matrix with singular values. The matrices $\mathbf{U}$ and $\mathbf{\Lambda}$ are obtained through singular value decomposition of $\mathbf{Y}$. The singular values larger than zero represent the corresponding sources so that the number of sources is determined and the matrices $\mathbf{U}$ and $\mathbf{\Lambda}$ are refined.

Second, consider the covariances with various time shifts. Making use of Eq. (2) and considering white noises $\mathbf{W}$, the covariance relation is given by

$$\mathbf{C_Z}(\tau) = \mathbf{T}\mathbf{C_Y}(\tau)\mathbf{T}^{\mathrm{T}} = \mathbf{T}\mathbf{H}\mathbf{C_F}(\tau)(\mathbf{T}\mathbf{H})^{\mathrm{T}} \tag{7}$$

where τ denotes time shift. Since the sources are independent of each other, the covariance matrix $\mathbf{C_F}$ is diagonal. By imposing singular value decomposition for the covariance matrix $\mathbf{C_Z}$ on the left-hand side of Eq. (7), a singular value matrix is obtained which is also diagonal. Thus, the so-called joint diagonalization is realized for the covariances with various time shifts, and a unitary matrix $\mathbf{V}$ is obtained, which yields

$$\mathbf{T}\mathbf{H} = \mathbf{V} \tag{8}$$

The joint diagonalization is to minimize the total absolute (or square) values of non-diagonal elements in the matrix $\mathbf{C_Z}$ for various time shifts by using the unitary matrix $\mathbf{V}$ (Belouchrani *et al*. 1997). Consequently, the mixture matrix is elicited as

$$\mathbf{H} = \mathbf{T}^{-1}\mathbf{V} = \mathbf{U}\mathbf{\Lambda}^{1/2}\mathbf{V} \tag{9}$$

In accordance with the optimal estimation, the sources are conditional expectations and determined by Eq. (1) as

$$\hat{\mathbf{F}}(t) = E[\mathbf{F}] = \mathbf{H}^{-1}E[\mathbf{Y}] = \mathbf{H}^{-1}\hat{\mathbf{Y}}(t) \tag{10}$$

where $E[\cdot]$ denotes the expectation, and the superscript -1 denotes the generalized inverse. $\hat{\mathbf{F}}$ is the estimated sources, while $\hat{\mathbf{Y}}$ is estimated from the measurements. In the above setting, the sources are normalized in unit variances. Making use of Eqs. (9) and (10), the blind sources can be separated where the sources are estimated in time domain and the mixture matrix is elicited using only the measurements. The mixture represents the dynamic characteristics of the unknown system between sources and measurements and can be used for abnormal feature identification as described in the next section.

3. SOSBS-based excitation separation and structural anomaly detection

Consider a multi-DOF structural or mechanical system with constant damping and stationary excitations, whose governing equation is

$$\mathbf{M}\ddot{\mathbf{X}} + \mathbf{C}\dot{\mathbf{X}} + \mathbf{K}\mathbf{X} = \mathbf{F}_p(t) \tag{11}$$

where $\mathbf{X}$ is the displacement vector, $\mathbf{F}_p$ is the excitation vector, and $\mathbf{M}$, $\mathbf{C}$, $\mathbf{K}$ are the mass, damping and stiffness matrices, respectively. The vibration modes can be non-orthogonal with respect to damping. Putting aside noises, the stationary excitations $\mathbf{F}_p$ consist of different ingredients as independent sources. The stationary responses can be expressed as

$$\begin{aligned}\mathbf{X}(t) &= \sum_{i=1}^{n} \mathbf{D}_i(\omega_i)\, G_i(\omega_i, t) \\ &\quad + \mathbf{W}(t) \triangleq \mathbf{H}\mathbf{F}(t) + \mathbf{W}(t)\end{aligned} \tag{12}$$

where ω_i is the *i*th excitation frequency, $\mathbf{D}_i$ is determined by the stationary solution to Eq. (11), and G_i corresponds to the harmonic excitation with certain phase difference. The stationary response of the system (11) under Gaussian noise excitation is a Gaussian process. The responses (12) pertaining to different DOFs within a certain time interval are expressed as the unknown mixture of excitations to the unknown system given in Eq. (1). The SOSBS method introduced in Section 2 will be applied to separate the excitations $\mathbf{F}$ and extract the mixture matrix $\mathbf{H}$ by using the noisy response measurements $\mathbf{X}$.

The mixture matrix $\mathbf{H}$ describes synthetically the dynamic relationship between each excitation and response, which contains constitutive relation or structural properties. For example, the *i*th column vector $\mathbf{D}_i$ in the matrix $\mathbf{H}$ is the absolute frequency response vector to the *i*th harmonic excitation. It is obtained by Eq. (11) as

$$\mathbf{D}_i = (\mathbf{K} + \mathrm{j}\omega_i\mathbf{C} - \omega_i^2\mathbf{M})^{-1}\mathbf{E}_i \tag{13}$$

where $\mathbf{E}_i$ is the excitation position vector and $\mathrm{j} = \sqrt{-1}$. It is seen that the mixture vector $\mathbf{D}_i$ depends strongly on the stiffness matrix $\mathbf{K}$. An alteration in stiffness will result in a change in the elements of the mixture matrix $\mathbf{H}$. The element most sensitive to the stiffness alteration exhibits a maximum change. For the stationary responses of the system (11) under stationary excitations, the power spectral

density can be expressed as

$$\mathbf{S_X}(\omega) = (\mathbf{K} + \mathrm{j}\omega\mathbf{C} - \omega^2\mathbf{M})^{-1}\mathbf{S}_{\mathbf{F}_p}^{1/2}(\omega)\left[\mathbf{S}_{\mathbf{F}_p}^{1/2}(\omega)\right]^{\mathrm{T}} (\mathbf{K} + \mathrm{j}\omega\mathbf{C} - \omega^2\mathbf{M})^{-\mathrm{T}} \quad (14)$$

where $\mathbf{S_F} = \mathbf{S}_{\mathbf{F}_p}^{1/2}(\omega)[\mathbf{S}_{\mathbf{F}_p}^{1/2}(\omega)]^{\mathrm{T}}$ and $\mathbf{S_X}$ are the power spectral density matrices of the excitations and responses, respectively, ω is the circular frequency, and the superscript T denotes the conjugate transpose. The response covariance matrix is

$$\mathbf{C_X}(\tau) = \frac{1}{2\pi}\int_{-\infty}^{+\infty}\mathbf{S_X}(\omega)\exp(\mathrm{j}\omega\tau)\mathrm{d}\omega \quad (15)$$

where τ denotes time shift which is different from time *t*. For a band-limited random process, the integral (15) can be approximated by finite differentiation. The covariance operation of the stationary responses (12) yields

$$\mathbf{C_X}(\tau) - \mathbf{C_W}(\tau) = \mathbf{H}\mathbf{C_F}(\tau)\mathbf{H}^{\mathrm{T}} \quad (16)$$

The response covariance matrix $\mathbf{C_X}$ can be converted into the form of the right-hand side of Eq. (16), and the mixture matrix $\mathbf{H}$ depends only on the absolute frequency response as expressed in Eq. (13). Hence, the mixture $\mathbf{H}$ describes the dynamic characteristics between each excitation and response.

Relative to the intact state, an alteration in system characteristics will directly result in a change in the elements of the mixture matrix $\mathbf{H}$. The elements with large change in their values indicate a local region of anomaly or damage, and the amplitude of the change expresses the degree of anomaly or damage. For example, the stiffness alteration $\Delta\mathbf{K}$ makes the mixture change in $\Delta\mathbf{D}_i$ and $\Delta\mathbf{H}$. The system anomaly or damage in terms of $\Delta\mathbf{K}$ can be diagnosed using the identified change in the elements (referred to as features hereafter) of the mixture matrix $\mathbf{H}$. The anomaly or damage index based on the features is thus defined as

$$J = \sum_i\sum_j \|\Delta\mathbf{H}_{ji}\|_m \quad (17)$$

where the mixture matrix $\mathbf{H}$ has been normalized, for example, with respect to the first element of each column, Δ denotes the difference, and $\|\cdot\|_m$ denotes the norm. The index for the norm with $m = \infty$ is

$$J = \max_{i,j}\{\Delta\mathbf{H}_{ji}\} \quad (18)$$

The index (17) or (18) can be used to quantify the system anomaly or damage.

4. Numerical simulation

4.1 Blind excitation separation and feature identification

To illustrate the applicability and effectiveness of the proposed method for blind excitation separation and mixture feature identification under periodic excitations, we consider a 3-DOF system expressed by Eq. (11) with dimensionless mass, stiffness, damping and excitations as follows

$$\begin{aligned}
&\mathbf{M} = \begin{bmatrix}1 & 0 & 0\\ 0 & 1 & 0\\ 0 & 0 & 1\end{bmatrix}\\
&\mathbf{K} = 10\times\begin{bmatrix}1.7 & -0.4 & -0.6\\ -0.4 & 1.3 & -0.8\\ -0.6 & -0.8 & 2.3\end{bmatrix}\\
&\mathbf{C} = 0.02\mathbf{M} + 0.01\mathbf{K}\\
&\mathbf{F}_p = \begin{bmatrix}f_1\sin(\omega_1 t + \theta_1)\\ f_2\sin(\omega_2 t + \theta_2)\\ 0\end{bmatrix}\\
&f_1 = 1.0,\quad f_2 = 0.5,\quad \omega_1 = 0.9,\quad \omega_2 = 0.5,\\
&\theta_1 = 0.3491,\quad \theta_2 = 0
\end{aligned} \quad (19)$$

where the mass matrix $\mathbf{M}$ has been unitized by the inverse of the original mass matrix, and the damping matrix $\mathbf{C}$ is given to satisfy the Rayleigh damping assumption. The natural circular frequencies of the system are obtained by the stiffness and mass matrices as 2.2361, 4.4065, 5.3463 rad/s. The stationary (steady-state) responses (X_1, X_2, X_3) are shown in Fig. 1. With the responses being the only measurements, the blind excitation separation and mixture feature extraction method proposed in the previous section is applied to obtain the separated excitations (F_1, F_2) as shown in Fig. 2. The results on the power spectral densities of the separated excitations validate that their frequencies are favorably in agreement with those of the true excitations. Furthermore, the mixture matrix $\mathbf{H}$ unit-normalized with the first elements in its columns is obtained as

$$\mathbf{H} = \begin{bmatrix}1 & 1\\ 0.6552 & 2.3382\\ 0.5060 & 1.0870\end{bmatrix} \quad (20)$$

while the mixture matrix $\mathbf{H}_0$ obtained by Eq. (13) is

$$\mathbf{H}_0 = \begin{bmatrix}1 & 1\\ 0.6632 & 2.4825\\ 0.5091 & 1.1367\end{bmatrix} \quad (21)$$

By comparison with Eq. (21), it is seen that the first column of the mixture matrix $\mathbf{H}$ obtained in Eq. (20) has better accuracy than the second column, and the second column of the mixture matrix $\mathbf{H}$ has a maximal relative error of 5.8%. The error is due to the relatively low amplitude of the second excitation. If the amplitude of the second excitation is increased to $f_2 = 1.0$, the extracted mixture matrix becomes

$$\mathbf{H} = \begin{bmatrix}1 & 1\\ 0.6587 & 2.4373\\ 0.5082 & 1.1202\end{bmatrix} \quad (22)$$

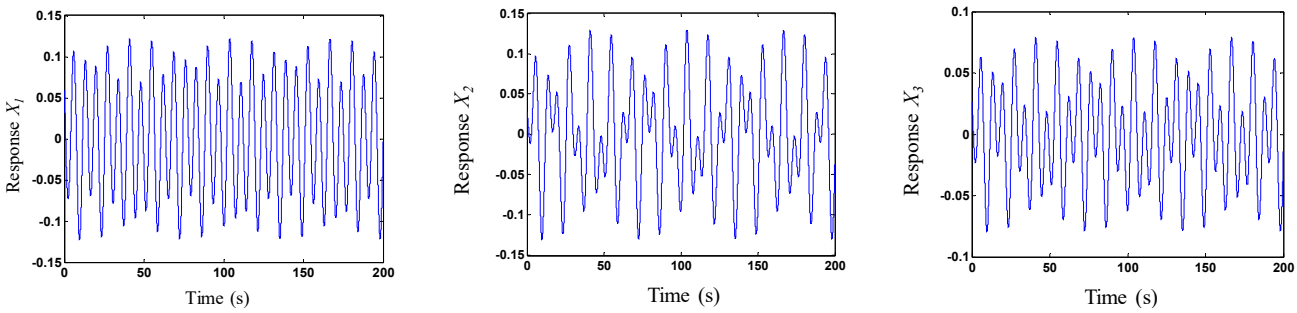

(a) (b) (c)

Fig. 1 System responses: (a) X_1; (b) X_2; and (c) X_3

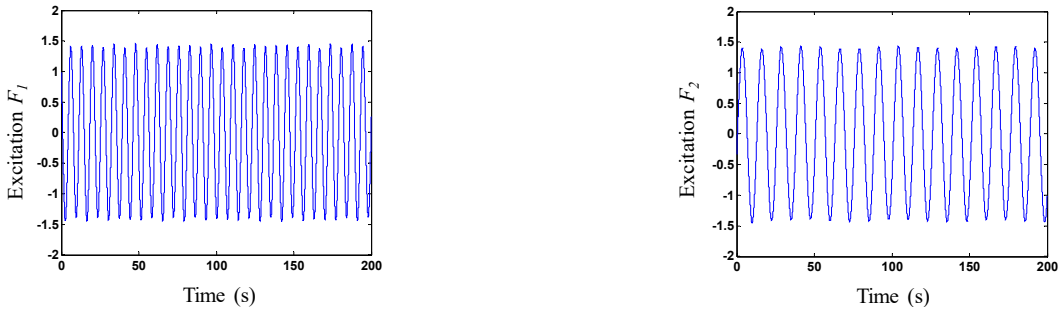

(a) (b)

Fig. 2 Identified excitations normalized with unit variances: (a) F_1; and (b) F_2

where the accuracy in both the first and second columns is ameliorated. Hence, the proposed method is competent for blind excitation separation and mixture feature extraction of the system. The extracted features will be used for system anomaly or damage diagnosis.

4.2 Mixture feature-based damage diagnosis

If damage results in a reduction of system stiffness, it will generate a change in mixture features. The mixture matrix **H** depicts synthetically the dynamic characteristics between each excitation and response and is reflective of alteration in system characteristics. In this study, different cases of stiffness reduction are considered to examine the feature variation. In the first case where the second diagonal stiffness element is reduced to $K_{22} = 10.4$ (20% relative reduction), the two columns of the resulting normalized mixture matrix **H** are shown in Fig. 3. The mixture matrix of the intact system is also shown for comparison. In Fig. 3(a), the second and third elements are smaller than the first element, indicating that the first excitation is acting on the first DOF. The second element has the largest variation as 39% increase [refer to Eq. (18)], implying a significant reduction of stiffness K_{22}. The relatively small variation shown in Fig. 3(b) cannot provide a strong evidence on stiffness reduction under the second excitation. In the second case, the third diagonal stiffness element is decreased to $K_{33} = 18.4$ (20% relative reduction). The two columns of the normalized mixture matrix **H** obtained in this case are shown in Fig. 4. The largest increase of 38% occurs in the third element of the first column, indicating a reduction in stiffness K_{33}. In the third case where the non-diagonal element K_{13} in the stiffness matrix is increased to $K_{13} = -4.8$ (20% relative reduction), the two columns of the obtained normalized mixture matrix **H** are shown in Fig. 5. This 20% reduction in K_{13} results in a decrease of 14% in the third element of the first column and an increase of 11% in the second element of the second column in the normalized mixture matrix **H**. Physically, this numerical example represents a 3-DOF system with three springs (k_1, k_2, k_3) supporting three masses (m_1, m_2, m_3) on a fixed base, respectively, and three springs (k_4, k_5, k_6) connecting the first and second masses (m_1 and m_2), the second and third masses (m_2 and m_3), and the first and third masses (m_1 and m_3), respectively, as shown in Fig. 6. As a result, a single-damage case which causes a reduction of stiffness in one of the three connecting springs will result in alteration in several elements (entries) of the stiffness matrix; moreover, a multiple-damage case which causes a reduction of stiffness in two or more springs must result in alteration in several elements (entries) of the stiffness matrix. For example, when the connecting spring k_6 is reduced from 6.0 to 4.8 due to damage, the non-diagonal element K_{13} in the stiffness matrix (19) is increased to $K_{13} = -4.8$ and $K_{31} = -4.8$ while the diagonal elements are decreased to $K_{11} = 15.8$ and $K_{33} = 21.8$. In this case, the relative reductions of the two columns of the obtained normalized mixture matrix **H** are $[0\ -3.6\%\ -7.2\%]^{\mathrm{T}}$ and $[0\ 1.2\%\ 1.4\%]^{\mathrm{T}}$. The increase of the first column in the normalized mixture matrix in relation to the first excitation on the first DOF of the system indicates an increasing variation from the first DOF to the third DOF, which is in conformance with the reduction of stiffness between the first and third DOFs.

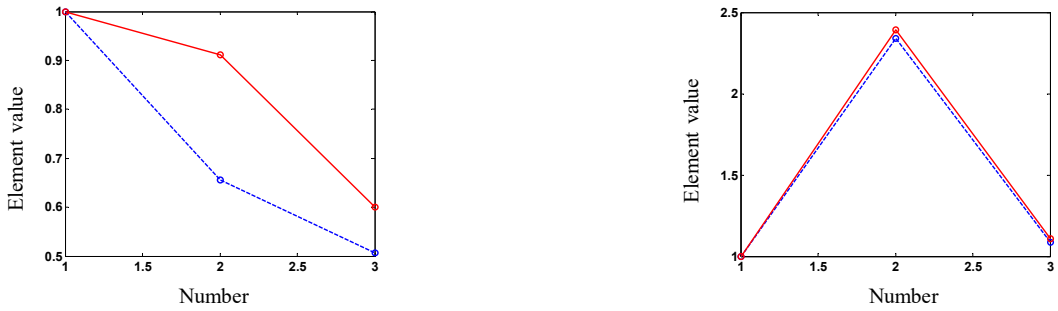

(a) (b)

Fig. 3 Elements of $\mathbf{H}$ in case of K_{22} reduced (blue dashed line: original; red solid line: 20% reduction in K_{22}): (a) 1st column; and (b) 2nd column

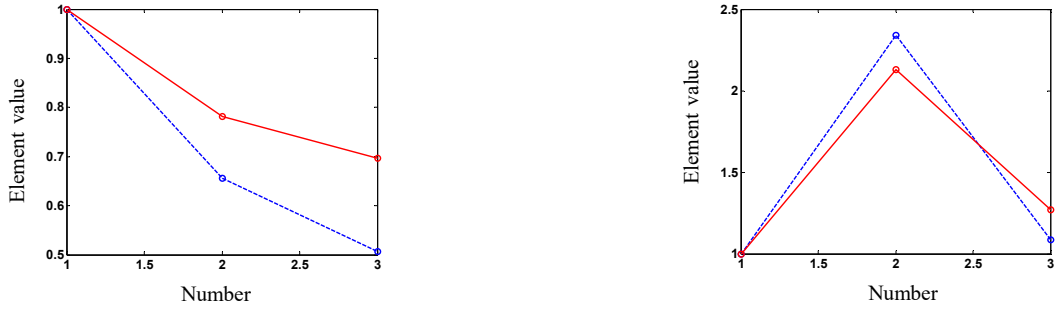

(a) (b)

Fig. 4 Elements of $\mathbf{H}$ in case of K_{33} reduced (blue dashed line: original; red solid line: 20% reduction in K_{33}): (a) 1st column; and (b) 2nd column

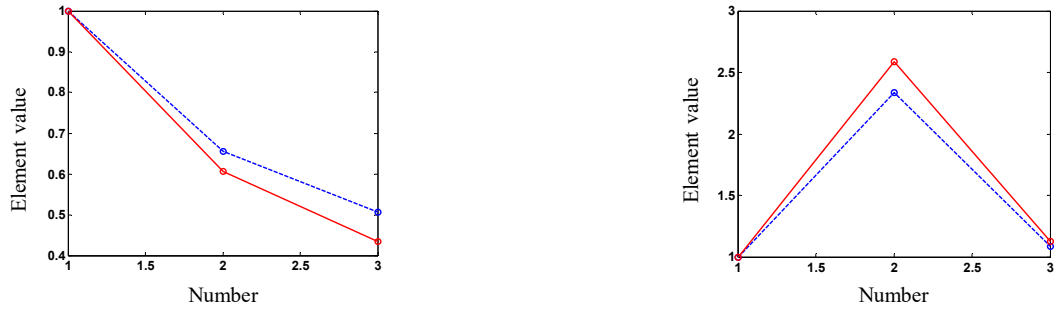

(a) (b)

Fig. 5 Elements of $\mathbf{H}$ in case of K_{13} reduced (blue dashed line: original; red solid line: 20% reduction in K_{13}): (a) 1st column; and (b) 2nd column

4.3 Effect of noise intensity on feature identification

Real-world measurement data are inevitably contaminated with noise. Random noise is introduced in this simulation study by considering it as a Gaussian white noise process, and the noise intensity is represented by signal-to-noise ratio (Kay 1984). Here the signal-to-noise ratio in dB is expressed as

$$SNR = 20\log_{10}\left(\sqrt{\frac{[\mathbf{C}_x]_{ii}}{[\mathbf{C}_\mathbf{W}]_{jj}}}\right) \tag{23}$$

In regard to different signal-to-noise ratios, the normalized mixture matrices are obtained using only the

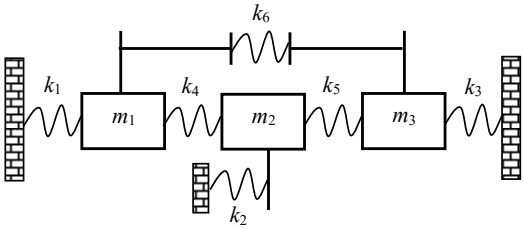

Fig. 6 Diagram of 3-DOF physical system

system responses. The second and third elements of the first column in the mixture matrix $\mathbf{H}$ versus the signal-to-noise ratio are shown in Figs. 7(a) and 7(b), respectively. The reference values of elements in the mixture matrix are given in Eq. (20). The second and third elements of the second

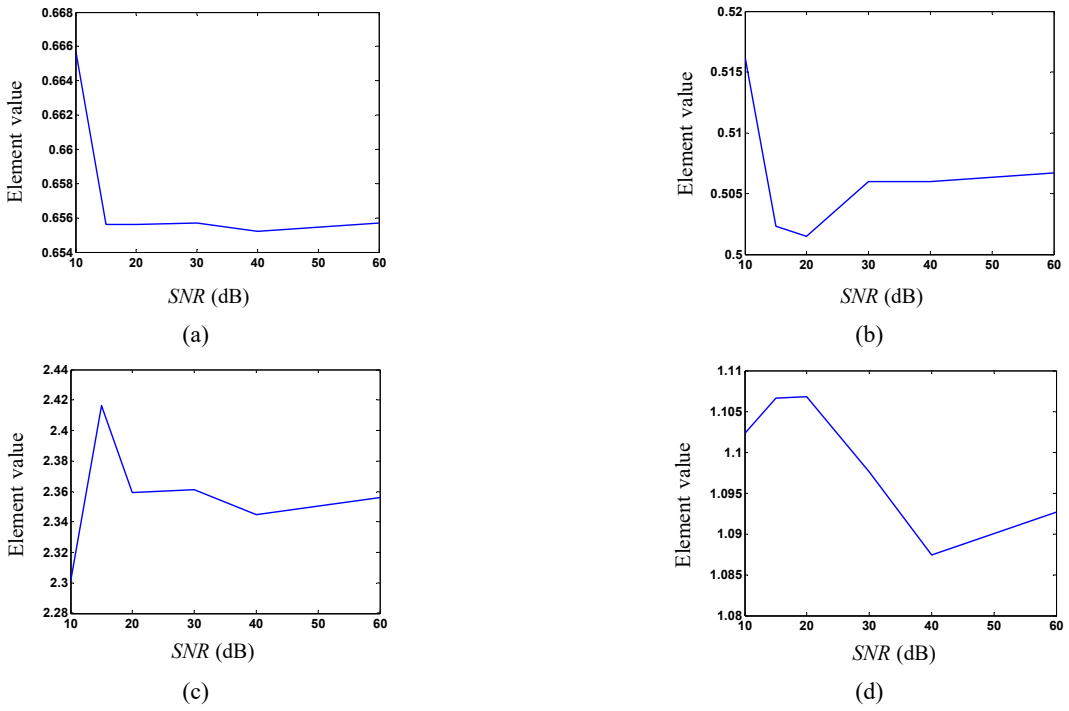

Fig. 7 Normalized values of elements in **H** versus SNR: (a) second element of first column; (b) third element of first column; (c) second element of second column; and (d) third element of second column

column in the mixture matrix **H** versus the signal-to-noise ratio are shown in Figs. 7(c) and 7(d), respectively. In the case of *SNR* < 30 dB, the second and third elements have maximum relative errors of 1.5% and 1.8%, respectively. Hence, the proposed blind excitation separation and structural feature identification method using second-order statistics is robust to measurement noise.

4.4 Feature identification under different excitation frequencies

We further observe the performance of the proposed method for mixture feature extraction under different excitation frequencies. The elements in the normalized mixture matrix **H** obtained under six sets of excitation frequencies are shown in Table 1, and the corresponding relative errors are obtained as provided in Table 2. It is observed that the identified mixture matrix has satisfactory accuracy over a wide range of excitation frequencies including those near the natural frequencies. The identified mixture matrix is reliable even with closely spaced excitation frequencies, but independent excitation sources may fail to be separated if the excitation frequencies are nearly identical. Except for the case of highly closed excitation frequencies, the proposed blind excitation separation and structural feature identification method using second-order statistics is robust to a wide range of excitation frequencies.

4.5 Feature identification under non-Rayleigh damping

Actual damping in a physical system may be complicated. There is the case of damping matrix which cannot be diagonalized by vibration modes. In this case, vibration modes are not independent of each other so that modal identification becomes unreliable. Consider the following non-diagonalizable and slow-varying damping matrix

$$\mathbf{C} = [1 + 0.2\sin(0.1t)]\begin{bmatrix} 0.15 & -0.04 & -0.06 \\ -0.04 & 0.1 & -0.07 \\ -0.06 & -0.07 & 0.2 \end{bmatrix} \quad (24)$$

In this case, the normalized mixture matrix **H** obtained by the proposed method is

$$\mathbf{H} = \begin{bmatrix} 1 & 1 \\ 0.6568 & 2.3540 \\ 0.5075 & 1.0937 \end{bmatrix} \quad (25)$$

and the true mixture matrix $\mathbf{H}_0$ with the average damping is

Table 1 Elements in mixture matrix **H** under different excitation frequencies

Frequencies (ω_1, ω_2) (rad/s)	Row 2, Column 1	Row 3, Column 1	Row 2, Column 2	Row 3, Column 2
(0.9, 0.5)	0.6548	0.5066	2.3401	1.0876
(0.9, 0.7)	0.6441	0.5028	2.4776	1.1470
(0.9, 2.1)	0.6497	0.5026	1.5922	1.0149
(0.9, 4.1)	0.6655	0.5149	0.4837	0.3518
(0.9, 4.9)	0.6591	0.5120	0.7078	0.6958
(0.9, 7.0)	0.6623	0.5092	14.7618	4.2310
(2.6, 6.0)	3.0059	1.8524	22.6438	12.0371
(12.0, 7.0)	0.0275	0.0471	13.9850	4.0394
(20.0, 30.0)	0.0102	0.0157	226.8222	2.0235

Table 2 Relative errors of elements in mixture matrix **H** under different excitation frequencies

Frequencies (ω_1, ω_2) (rad/s)	Row 2, Column 1	Row 3, Column 1	Row 2, Column 2	Row 3, Column 2
(0.9, 0.5)	1.1%	0.5%	5.7%	4.3%
(0.9, 0.7)	2.3%	1.2%	1.9%	1.4%
(0.9, 2.1)	1.9%	1.3%	1.7%	0.4%
(0.9, 4.1)	0.5%	1.1%	0.8%	0.3%
(0.9, 4.9)	0.5%	0.6%	3.4%	6.7%
(0.9, 7.0)	0.0%	0.0%	5.4%	3.7%
(2.6, 6.0)	0.5%	0.7%	2.9%	8.7%
(12.0, 7.0)	1.1%	2.1%	0.2%	1.0%
(20.0, 30.0)	0.0%	0.2%	5.8%	0.1%

$$\mathbf{H}_0 = \begin{bmatrix} 1 & 1 \\ 0.6632 & 2.4825 \\ 0.5092 & 1.1367 \end{bmatrix} \tag{26}$$

It is seen by comparing Eqs. (25) and (26) that the first column of the mixture matrix **H** has better accuracy while the second column of the mixture matrix **H** has the maximum relative difference of 5.2% which is much less than the damage-induced change in the mixture features as provided in Sub-section 4.2. Therefore, the proposed blind excitation separation and structural feature identification method using second-order statistics performs satisfactorily even when the real damping is non-diagonalized by vibration modes but varies slowly with time.

4.6 Feature identification under simultaneously random and periodic excitations

Random excitation has a wide frequency band and would result in complex system response. The relationship between random excitation and response and the corresponding mixture are dependent on the characteristics of excitation spectral density. However, in the case of simultaneously random and periodic excitations, the effective separation of periodic excitation is still possible when the random excitation can be considered as ambient noise. Consider the second excitation F_{p2} in Eq. (19) to be random with its power spectral density

$$S_f(\omega) = \frac{1 + 4\zeta_g^2(\omega/\omega_g)^2}{\left[1 - (\omega/\omega_g)^2\right]^2 + 4\zeta_g^2(\omega/\omega_g)^2} S_0 \tag{27}$$

where S_0 = 0.1, ζ_g = 0.3 and ω_g = 23 rad/s. The system responses (X_1, X_2, X_3) are shown in Figs. 8(a), 8(b) and 8(c). By the proposed method, the separated periodic and random excitations (F_1, F_2) are obtained as shown in Figs. 9(a) and 9(b). The periodic excitation has been successfully extracted from the random mixed sources. The normalized mixture vector $\mathbf{H}_1$ pertaining to the periodic excitation is obtained as

$$\mathbf{H}_1 = [1 \quad 0.6857 \quad 0.5227]^T \tag{28}$$

while the corresponding mixture vector $\mathbf{H}_{01}$ obtained in the absence of random excitation is

$$\mathbf{H}_{01} = [1 \quad 0.6623 \quad 0.5091]^T \tag{29}$$

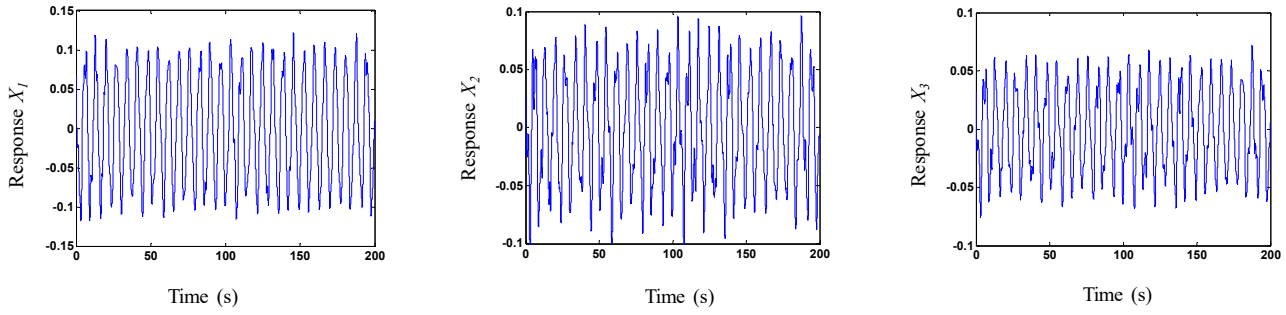

(a) (b) (c)

Fig. 8 System responses: (a) X_1; (b) X_2; and (c) X_3

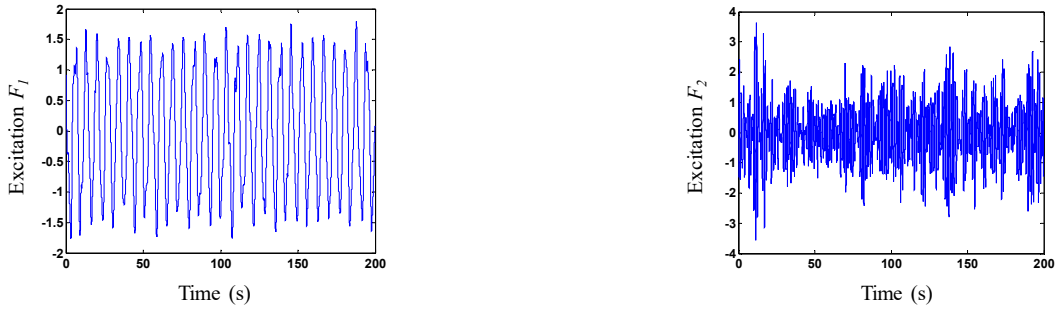

(a) (b)

Fig. 9 Identified excitations normalized with unit variance: (a) F_1; and (b) F_2

Fig. 10 Five-story steel frame model

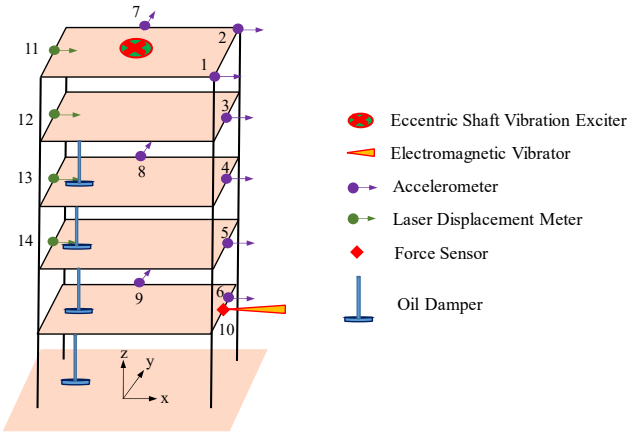

Fig. 11 Layout of sensors and vibration exciters

It is seen by comparing Eqs. (28) and (29) that the identified mixture pertaining to the periodic excitation is very close to that obtained in the absence of random excitation. Hence, the proposed blind excitation separation and structural feature identification method using second-order statistics is workable for extracting periodic excitation and its mixture features from relatively light and band-limited random excitation mixed sources.

5. Experimental verification

5.1 Structural model and experimental setup

To experimentally verify the performance of the proposed blind excitation separation and abnormal feature identification method using second-order statistics, a 5-story shear-type frame is built, as shown in Fig. 10. The frame structure consists of five steel floors with size of 600 mm × 400 mm × 15 mm and four steel columns with a rectangular cross section of 50 mm × 6 mm each. Each floor (plate) is firmly welded perpendicular to the four columns. Each story has a height of 200 mm and the total height of the model is 1000 mm. Oil dampers are designed and installed between adjacent floors to make the structural damping close to that in an actual structure. With the excitations applied in the horizontal x-direction, only the floor motion in the x-direction is taken into account while that in the y-direction is ignored due to the relatively large stiffness in the y-direction. In practice, a complex large-scale structure may suffer multiple excitations in different directions, and multiaxial sensors need to be deployed to capture three-dimensional vibration responses. Although only excitations and responses in the x-direction are considered in this experimental study, the proposed method

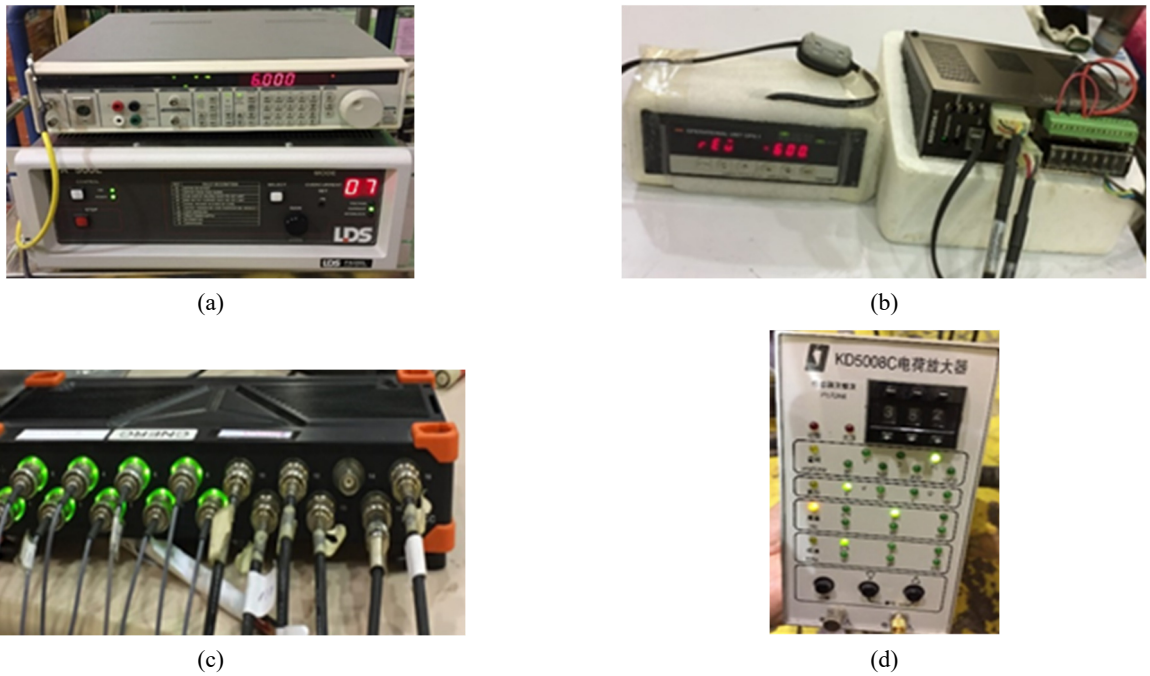

(a) (b)

(c) (d)

Fig. 12 Instruments used in the experiment: (a) signal generator and power amplifier; (b) controller of eccentric shaft vibration exciter; (c) signal acquisition device; and (d) charge amplifier for force sensor

Table 3 Specifications of instruments and sensors used in the experiment

Instrument/Sensor	Model type	Specifications
Electromagnetic vibrator	LDS® V406, Brüel & Kjær, Denmark	Sin force peak 98 N; Max acceleration sine peak 100g; Usable frequency range 5 Hz - 9 kHz
Power amplifier	LDS® PA500L, Brüel & Kjær, Denmark	Paired with LDS® V406, producing a Sin force peak 196 N
Signal generator	Model DS360 Ultra Low Distortion Function Generator, Stanford Research System, USA	Usable frequency range 0.1 Hz - 200 kHz
Eccentric shaft vibration exciter	BXD120A-C, Oriental Motor, Japan	Sin force peak 60 N; Usable frequency range 0.1 Hz - 100 Hz
Signal acquisition instrument	SIRIUS, Dewesoft, Slovenia	16 channels; Maximum sample rate 200 kHz
Charge amplifier	KD5008C, Kedong, China	Usable frequency range 0.1 Hz - 100 kHz
Laser displacement meter	LK-500, Keyence Corporation of America, USA	Measuring range -250 to +500 mm; Accuracy ±0.05% of full scale; Maximum sample rate 1000 Hz
Accelerometer	TYPE 4533-B-002, Brüel & Kjær, Denmark	Maximum operational level 714 g; Sensitivity 50 mV/ms^{-2}; Usable frequency range 0.2 Hz - 12800 Hz

is applicable to the extraction of excitation sources in different directions when three-dimensional dynamic responses are measured.

Two exciters are used in the experiment: an eccentric shaft vibration exciter placed on the top floor and an electromagnetic vibrator positioned at the first floor. Four laser displacement meters, nine uniaxial accelerometers and one force sensor are deployed on the structural model as shown in Fig. 11. The test system includes an electromagnetic vibrator (LDS® V406, Brüel & Kjær, Denmark), a signal generator (Model DS360 Ultra Low Distortion Function Generator, Stanford Research System, USA), a power amplifier (LDS® PA500L, Brüel & Kjær, Denmark), an eccentric shaft vibration exciter with controller (BXD120A-C, Oriental Motor, Japan), a signal acquisition instrument (SIRIUS, Dewesoft, Slovenia), and a charge amplifier (KD5008C, Kedong, China) as illustrated in Fig. 12. The structural model is excited by the vibrator and exciter with specific frequencies. The displacement response at each floor is measured by the laser displacement meter (LK-500, Keyence Corporation of America, USA); and meanwhile, the acceleration response at each floor is recorded by the accelerometer (TYPE 4533-B-002, Brüel & Kjær, Denmark). The specifications of the instruments and sensors used in the experiment can be found in Table 3. The sampling rate for all the measurands is set as 600 Hz. The structural responses collected will be utilized for modal identification, blind excitation separation and abnormal feature extraction to examine the performance of the proposed method in damage diagnosis.

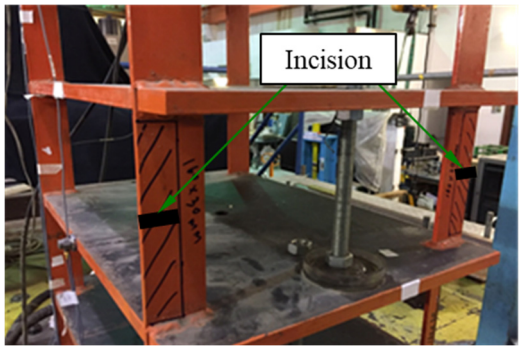

Fig. 13 Structural damage incurred

5.2 Damage scenarios and modal properties

Structural damage generally leads to a reduction in structural stiffness. Here, the stiffness reduction of steel columns is introduced to simulate damage to the frame structure, where the cross sections of two columns on the right side are partially cut off to reduce the bending stiffness as shown in Fig. 13. In the experimental study, three damaged scenarios together with the undamaged (intact) state are considered. The undamaged structure is denoted as

Table 4 Modal frequencies and their relative variations between undamaged and damaged states

Mode No.	Case 1 (intact)	Case 2 (damage at 2nd story)		Case 3 (damage at 2nd and 3rd stories)		Case 4 (damage at 1st, 2nd and 3rd stories)	
	Frequency (Hz)	Frequency (Hz)	Change (%)	Frequency (Hz)	Change (%)	Frequency (Hz)	Change (%)
1	8.79	8.50	3.30	8.31	5.46	7.91	10.01
2	26.07	25.71	1.38	24.61	5.60	24.17	7.29
3	42.48	40.21	5.34	39.99	5.86	39.70	6.54
4	56.40	55.39	1.79	54.20	3.90	51.27	9.09
5	66.65	63.21	5.16	60.79	8.79	57.71	13.41

Case 1, and Cases 2 to 4 correspond to three damaged cases: (i) story stiffness reduction of 30% at the 2nd story (Case 2); (ii) story stiffness reduction of 30% at the 2nd and 3rd stories simultaneously (Case 3), and (iii) story stiffness reduction of 30% at the 1st, 2nd and 3rd stories simultaneously (Case 4). The damage severity increases gradually from Case 1 to Case 4.

The dynamic characteristics of the frame structure in Cases 1 to 4 are firstly identified by hammer tests, from which the modal properties including modal frequencies and mode shapes are estimated. The first five modal frequencies in the x-direction and their relative variations between the damaged and undamaged states are provided in Table 4. The modal frequency of each mode decreases with the increase of damage severity, and its maximum relative reduction is 13.41% in the fifth mode, followed by the first mode with 10.01% reduction. Fig. 14 shows the first five bending mode shapes of the undamaged and damaged structures in the x-direction, where the amplitude of each mode is normalized to unit. It is seen that the change of mode shapes from undamaged to damaged states is insignificant. Accurate identification of mode shapes is in general more difficult than modal frequencies, especially for high-order modes.

5.3 Results of feature identification

To examine the performance of the proposed blind excitation separation and abnormal feature identification method, two periodic excitations with different frequencies and amplitudes are concurrently applied to the frame structure on the 1st and 5th floors. The two periodic excitations are expressed as

$$F_i = f_i \sin(2\pi\alpha_i t + \theta_i) \qquad i = 1,2 \tag{30}$$

where f_i's are the excitation amplitudes, α_i's are the excitation frequencies in Hz, and θ_i's are the phase angles. The periodic force F_1 acting on the 1st floor is generated by the electromagnetic vibrator, and the periodic force F_2 acting on the 5th floor is generated by the eccentric shaft vibration exciter. In this study, five sets of excitations with various frequencies ((2 Hz, 10 Hz), (3 Hz, 10 Hz), (4 Hz, 10 Hz), (2 Hz, 10.5 Hz) and (3 Hz, 10.5 Hz)) and amplitudes are considered in both healthy case (Case 1) and damaged cases (Case 2, Case 3 and Case 4), as shown in Tables 5 to 8.

Under the two excitations with frequencies of 2 Hz and 10 Hz, the displacement responses of the undamaged (intact) structure (Case 1) are first measured. The response time histories at the 2nd, 3rd and 4th floors and their power spectral densities (PSDs) are shown in Fig. 15. The PSDs of the responses display clearly the two excitation frequencies of 2 Hz and 10 Hz. Using only the measured displacement dynamic responses at the three floors, the two periodic excitations as unknowns are accurately separated by the proposed method. The extracted excitations versus time and their PSDs are shown in Fig. 16. The PSDs illustrate that

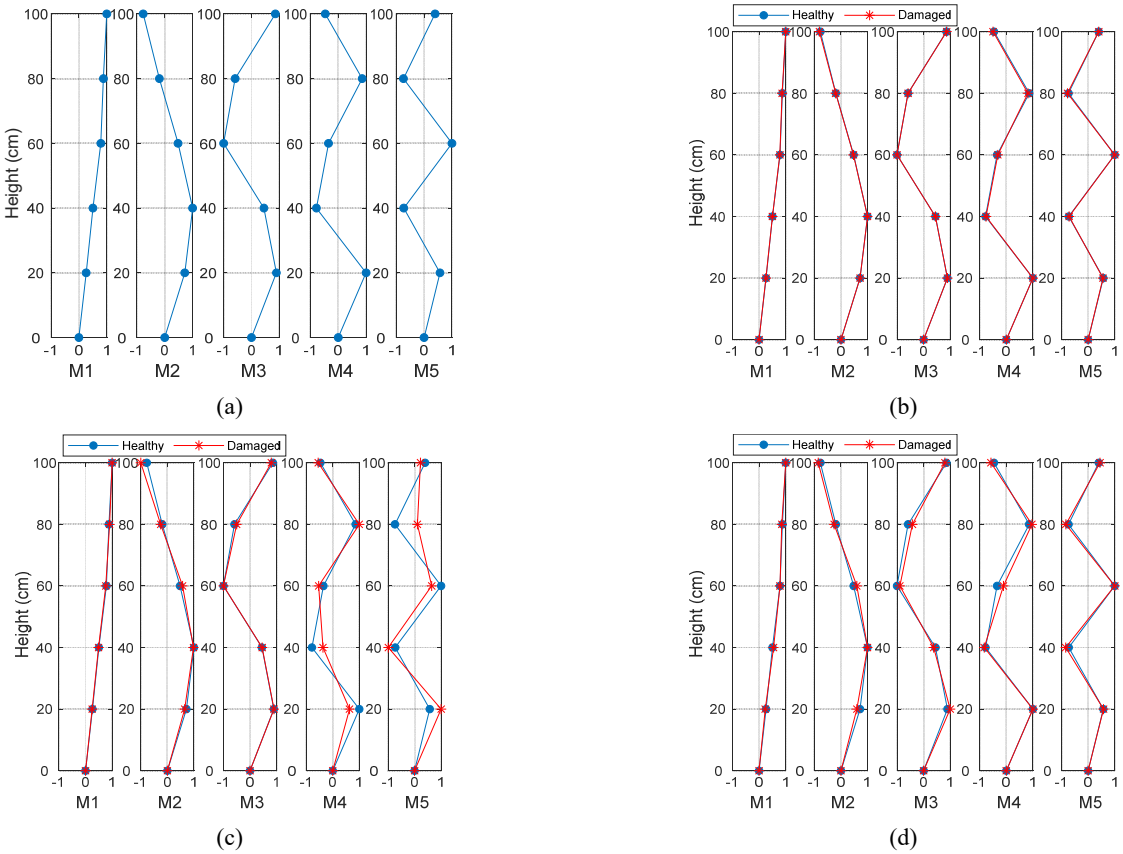

Fig. 14 Modal shapes of tested structure in healthy and damaged states: (a) Case 1 – healthy; (b) Case 2 – damaged; (b) Case 3 – damaged; (b) Case 4 – damaged

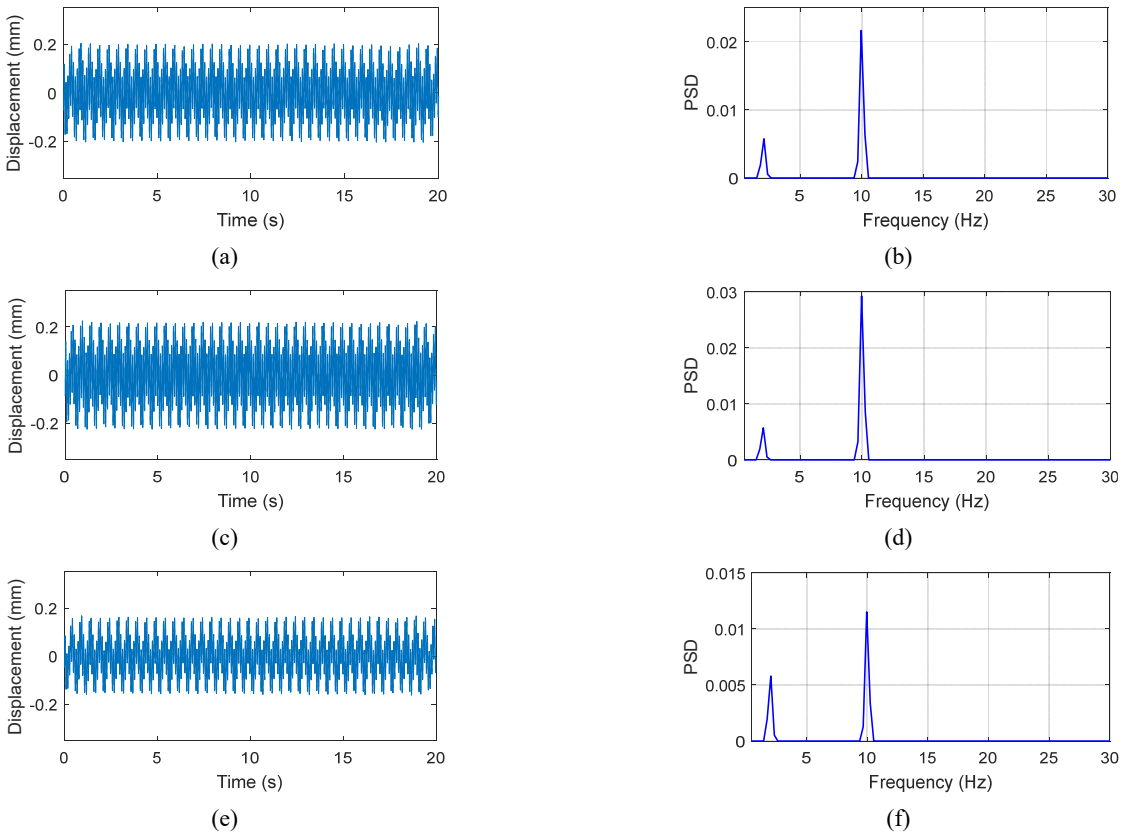

Fig. 15 Measured displacement responses and corresponding PSDs (excitation frequencies: 2 Hz and 10 Hz) in Case 1 (healthy)

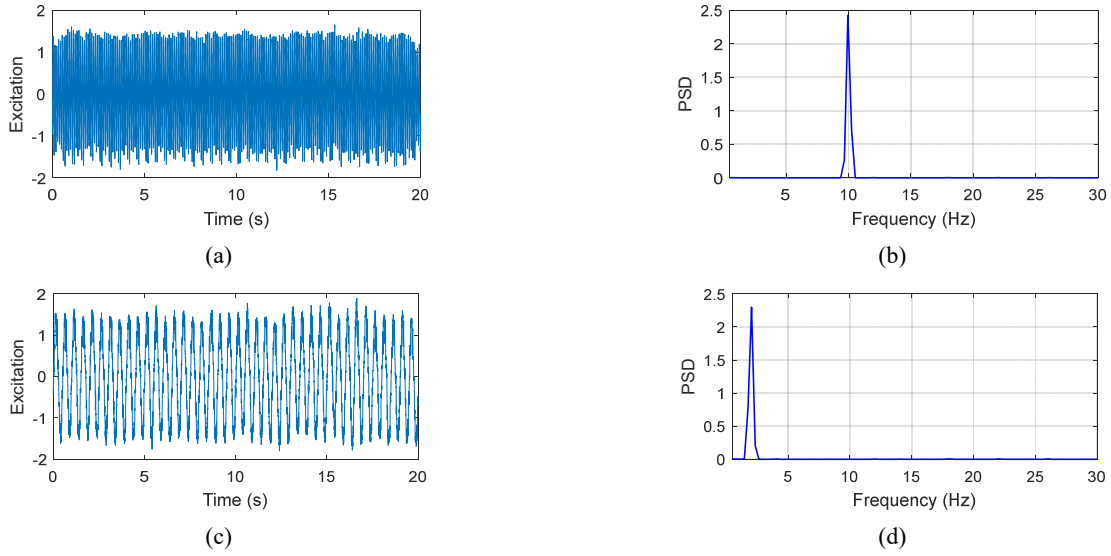

Fig. 16 Extracted excitations normalized with unit variance and corresponding PSDs (excitation frequencies: 2 Hz and 10 Hz) in Case 1 (healthy)

the two excitations have frequencies of 2 Hz and 10 Hz, respectively, being exactly the same as the real excitation frequencies. Then more excitations with various frequencies and amplitudes are considered in the experiment. For each excitation case, the mixture matrix $\mathbf{H}$ normalized with unit first elements is extracted using the measured displacement responses at the three floors. The elements in the second and third rows of the first and second columns in the mixture matrix $\mathbf{H}$ for different excitation cases are listed in Table 5. It is seen that the identified mixture matrix has good stability under various excitations, demonstrating the robustness of the proposed blind excitation separation and structural feature extraction method.

Next, the structure in damaged states (Cases 2 to 4) is tested under various excitations. Fig. 17 shows the displacement response time histories at the 2nd, 3rd and 4th

Table 5 Elements in mixture matrix **H** identified under various excitations in Case 1 (healthy)

Frequencies (α_1, α_2) (Hz)	(f_1, f_2)	Row 2, Column 1	Row 3, Column 1	Row 2, Column 2	Row 3, Column 2
(2, 10)	(88.41, 15.15)	1.1638	0.7287	0.9941	1.0084
(3, 10)	(111.40, 15.15)	1.1620	0.7181	0.9983	0.9871
(4, 10)	(123.56, 15.15)	1.1589	0.7124	1.0164	0.9590
(2, 10.5)	(102.21, 16.70)	1.1609	0.7079	0.9947	0.9763
(3, 10.5)	(124.88, 16.70)	1.1613	0.7125	1.0072	0.9602
Mean value		1.1614	0.7159	1.0021	0.9782

floors and their PSDs in Case 2 (damage at the 2nd story) when the two excitations have frequencies of 4 Hz and 10 Hz. Using only the measured displacement responses at the three floors, the two periodic excitations as unknowns are accurately separated by the proposed method. The extracted excitations versus time and their PSDs are shown in Fig. 18. The PSDs illustrate that the two excitations have frequencies of 4 Hz and 10 Hz, respectively, exactly the same as the real excitation frequencies. For excitations with various frequencies and amplitudes, the mixture matrix **H** normalized with unit first elements is extracted using the measured displacement responses at the three floors. The elements in the second and third rows of the first and second columns in the mixture matrix **H** for different excitations are listed in Table 6. The element of the first column and third row in **H** has the maximum mean variation of 8.03% in comparison with Case 1 (intact), where the first column indicates the excitation F_1 at the first floor and the third row indicates the response of the third floor. The element with the second largest variation (3.02%) occurs at the first column and second row. Thus, the two elements with the largest relative variations in the mixture matrix indicate a stiffness reduction between the 2nd and 3rd floors. Also, the maximum relative variation in the mixture matrix **H** is larger than that of the modal frequencies given in Table 4, indicating that **H** is quite sensitive to structural damage in addition to locating the region of damage. In fact, modal frequencies represent global dynamic characteristics of a structure and oftentimes are insensitive to local damage, but responses are strongly contingent on structural conditions between excitation and measurement points and are more sensitive to local damage. The mixture features that represent local structural dynamic characteristics obtained by the proposed method using second-order statistics of the measured responses can be effective to indicate structural damage. The above results demonstrate the capability of the proposed method for abnormal feature identification or damage diagnosis.

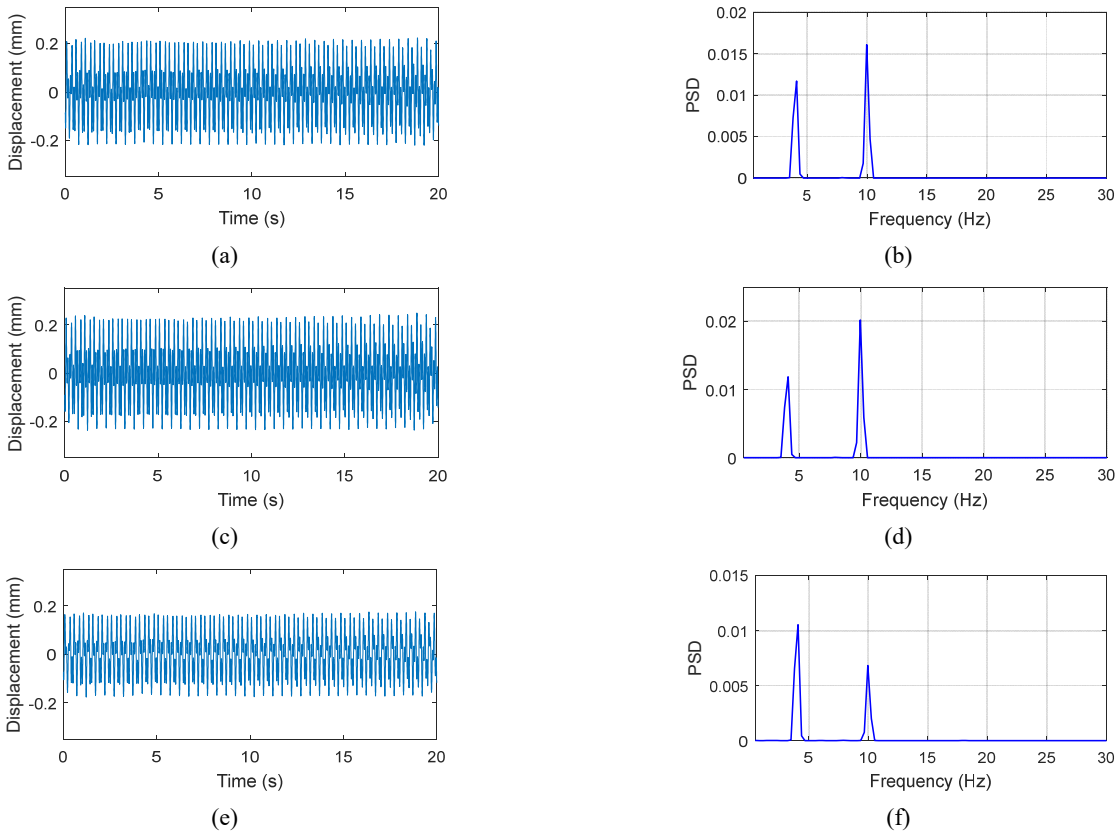

Fig. 17 Measured displacement responses and corresponding PSDs (excitation frequencies: 4 Hz and 10 Hz) in Case 2 (damaged)

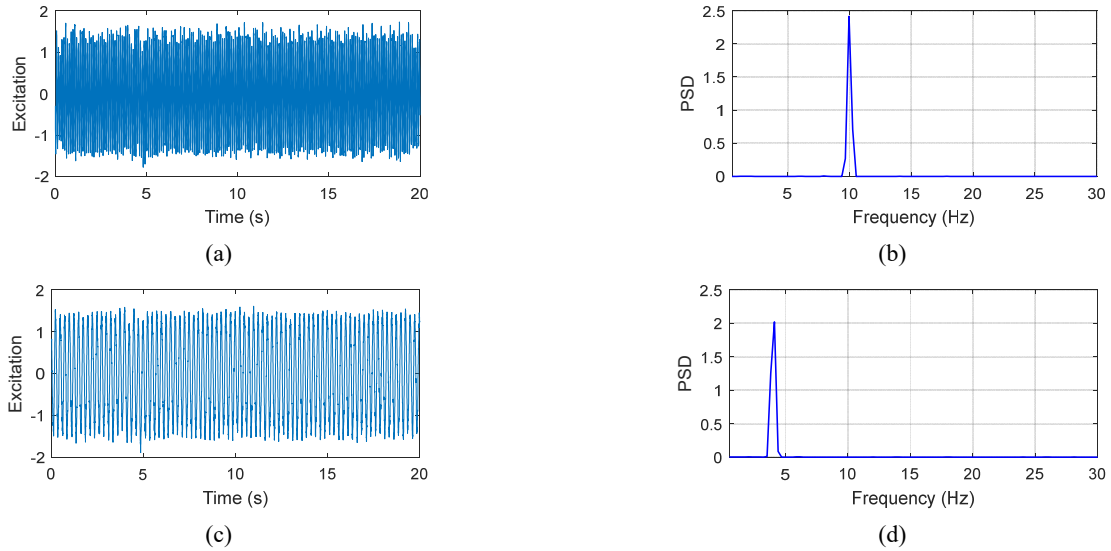

Fig. 18 Extracted excitations normalized with unit variance and corresponding PSDs (excitation frequencies: 4 Hz and 10 Hz) in Case 2 (damaged)

Table 6 Elements in mixture matrix **H** identified under various excitations in Case 2 (damaged)

Frequencies (α_1, α_2) (Hz)	(f_1, f_2)	Row 2, Column 1	Row 3, Column 1	Row 2, Column 2	Row 3, Column 2
(2, 10)	(98.85, 15.15)	1.1290	0.6595	0.9796	1.0116
(3, 10)	(108.38, 15.15)	1.1260	0.6563	0.9874	0.9875
(4, 10)	(112.45, 15.15)	1.1223	0.6512	1.0039	0.9503
(2, 10.5)	(114.40, 16.70)	1.1233	0.6649	1.0263	0.9736
(3, 10.5)	(116.90, 16.70)	1.1308	0.6600	1.0406	0.9819
Mean value		1.1263	0.6584	1.0076	0.9810
Relative variation		3.02%	8.03%	0.55%	0.29%

Table 7 Elements in mixture matrix **H** identified under various excitations in Case 3 (damaged)

Frequencies (α_1, α_2) (Hz)	(f_1, f_2)	Row 2, Column 1	Row 3, Column 1	Row 2, Column 2	Row 3, Column 2
(2, 10)	(97.43, 15.15)	1.2633	0.6980	1.0472	1.0585
(3, 10)	(106.76, 15.15)	1.2633	0.6979	1.0593	1.0331
(4, 10)	(103.24, 15.15)	1.2528	0.6935	1.0790	0.9912
(2, 10.5)	(94.95, 16.70)	1.2671	0.7153	1.0619	1.0628
(3, 10.5)	(100.00, 16.70)	1.2628	0.7062	1.0722	1.0367
Mean value		1.2619	0.7022	1.0639	1.0365
Relative variation		8.65%	1.91%	6.17%	6.95%

For Case 3 (damage at the 2nd and 3rd stories) and Case 4 (damage at the 1st, 2nd and 3rd stories), the displacement responses at the 2nd, 3rd and 4th floors are collected again under excitations with various frequencies and amplitudes. Using only the measured displacement responses at the three floors, the two periodic excitations are accurately separated and the mixture matrix **H** normalized with unit first elements is extracted by the proposed method. The elements of the second and third rows of the first and second columns in the mixture matrix **H** for different excitations are listed in Tables 7 and 8. In Table 7, the elements of the first column in **H** have the maximum mean variation of 8.65% in the second row and the elements of the second column have the maximum mean variation of 6.95% in the third row, indicating that damage occurs at the 2nd and 3rd stories. In Table 8, the element of the first column and second row in **H** has the maximum mean variation of 14.85% and three elements change more than

Table 8 Elements in mixture matrix **H** identified under various excitations in Case 4 (damaged)

Frequencies (α_1, α_2) (Hz)	(f_1, f_2)	Row 2, Column 1	Row 3, Column 1	Row 2, Column 2	Row 3, Column 2
(2, 10)	(95.49, 15.15)	0.9920	0.6126	0.8760	0.8794
(3, 10)	(106.27, 15.15)	0.9959	0.6146	0.8954	0.8619
(4, 10)	(97.67, 15.15)	1.0057	0.6146	0.9157	0.8353
(2, 10.5)	(98.16, 16.70)	0.9747	0.6187	0.8856	0.8877
(3, 10.5)	(97.79, 16.70)	0.9760	0.6199	0.8979	0.8703
Mean value		0.9889	0.6161	0.8941	0.8670
Relative variation		14.85%	13.53%	11.23%	9.71%

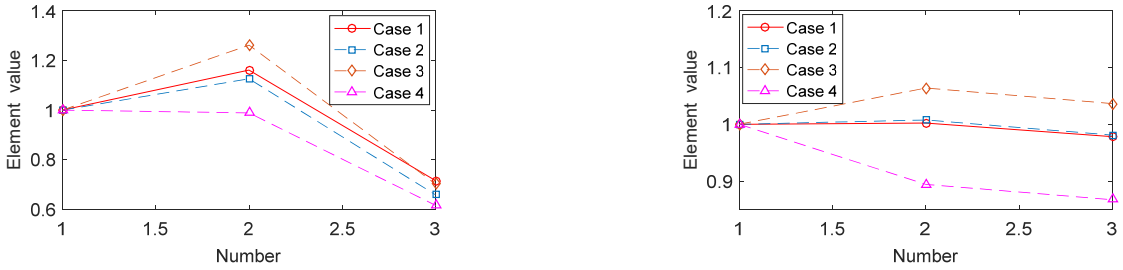

Fig. 19 Comparison of mixture matrix elements for different cases: (a) first column elements in **H**; and (b) second column elements in **H**

10% in comparison with Case 1 (intact), which shows stiffness reduction from the 1st story to the 3rd story. The maximum relative variation in **H** is larger than that of modal frequencies given in Table 4, implying that **H** is more sensitive to stiffness reduction than modal frequencies. Figs. 19(a) and 19(b) show a comparison of elements in the first and second columns of **H** between undamaged and damaged cases. It is seen that the variation of element values in the mixture matrix **H** increases with the damage severity (total stiffness reduction) and damage location/region can be determined through a synthetic analysis of the element variations.

6. Conclusions

In this study, a data-driven blind excitation separation and structural feature extraction method using only second-order statistics of measured responses was proposed. The mixture matrix that represents structural dynamic characteristics was extracted and used for abnormal feature identification or damage diagnosis.

The proposed method has been examined by numerical simulation and experiment study. The numerical simulation results for a 3-DOF system show that: (i) the extracted mixture features are sensitive to stiffness reduction and thus damage can be diagnosed by identifying variation in the features deviating from the intact structure; (ii) the proposed method is quite robust to measurement noise and yields consistent feature extraction under a wide range of excitation frequencies; (iii) it performs satisfactorily for blind excitation separation and feature extraction even when the real damping is non-diagonalized by vibration modes but varies slowly with time; and (iv) it is workable for periodic excitation separation from relatively light and band-limited random excitation mixed sources. The experimental study of a 5-story physical structure under various damaged states show that: (i) the extracted mixture matrix reflecting structural anomaly or damage has good stability under various excitations; and (ii) the extracted mixture matrix is more sensitive to stiffness reduction than modal frequencies, enabling more reliable damage diagnosis.

As a future research direction, the proposed blind excitation separation and structural feature extraction method using only response measurements will be extended and explored to make it workable for structures under other kinds of excitations, such as non-stationary wide-band random excitations.

Acknowledgments

The work described in this paper was partially supported by a grant from the Research Grants Council of the Hong Kong Special Administrative Region, China (Grant No. PolyU 152767/16E) and in part by a grant from the National Science Foundation of China (Grant No. 12072312). The authors would also like to appreciate the funding support by the Innovation and Technology Commission of the Hong Kong SAR Government (Grant No. K-BBY1).

References

Abed-Meraim, K., Xiang, Y., Manton, J.H. and Hua, Y. (2001), "Blind source-separation using second-order cyclostationary statistics", *IEEE Transact. Signal Process.*, **49**(4), 694-701. https://doi.org/10.1109/78.912913

Antoni, J. and Chauhan, S. (2013), "A study and extension of second-order blind source separation to operational modal analysis", *J. Sound Vib.*, **332**(4), 1079-1106. https://doi.org/10.1016/j.jsv.2012.09.016

Beck, J.L. and Katafygiotis, L.S. (1998), "Updating models and their uncertainties. I: Bayesian statistical framework", *J. Eng. Mech.*, **124**(4), 455-461. https://doi.org/10.1061/(ASCE)0733-9399(1998)124:4(455)

Belouchrani, A. and Amin, M.G. (1998), "Blind source separation based on time-frequency signal representations", *IEEE Transact. Signal Process.*, **46**(11), 2888-2897. https://doi.org/10.1109/78.726803

Belouchrani, A., Abed-Meraim, K., Cardoso, J.F. and Moulines, E. (1997), "A blind source separation technique using second-order statistics", *IEEE Transact. Signal Process.*, **45**(2), 434-444. https://doi.org/10.1109/78.554307

Bouguerriou, N., Haritopoulos, M., Capdessus, C. and Allam, L. (2005), "Novel cyclostationarity-based blind source separation algorithm using second order statistical properties: theory and application to the bearing defect diagnosis", *Mech. Syst. Signal Process.*, **19**(6), 1260-1281. https://doi.org/10.1016/j.ymssp.2005.07.007

Brewick, P.T. and Smyth, A.W. (2017), "Increasing the efficiency and efficacy of second-order blind identification (SOBI) methods", *Struct. Control Health Monitor.*, **24**(6), e1921. https://doi.org/10.1002/stc.1921

Brownjohn, J.M., De Stefano, A., Xu, Y.L., Wenzel, H. and Aktan, A.E. (2011), "Vibration-based monitoring of civil infrastructure: challenges and successes", *J. Civil Struct. Health Monitor.*, **1**(3-4), 79-95. https://doi.org/10.1007/s13349-011-0009-5

Bull, L.A., Worden, K., Fuentes, R., Manson, G., Cross, E.J. and Dervilis, N. (2019), "Outlier ensembles: a robust method for damage detection and unsupervised feature extraction from high-dimensional data", *J. Sound Vib.*, **453**, 126-150. https://doi.org/10.1016/j.jsv.2019.03.025

Carden, E.P. and Fanning, P. (2004), "Vibration based condition monitoring: a review", *Struct. Health Monitor.*, **3**(4), 355-377. https://doi.org/10.1177/1475921704047500

Ciambella, J., Pau, A. and Vestroni, F. (2019), "Modal curvature-based damage localization in weakly damaged continuous beams", *Mech. Syst. Signal Process.*, **121**, 171-182. https://doi.org/10.1016/j.ymssp.2018.11.012

Deraemaeker, A. and Worden, K. (2010), *New Trends in Vibration Based Structural Health Monitoring*, Springer, New York, USA.

Dessi, D. and Camerlengo, G. (2015), "Damage identification techniques via modal curvature analysis: overview and comparison", *Mech. Syst. Signal Process.*, **52**, 181-205. https://doi.org/10.1016/j.ymssp.2014.05.031

Fan, W. and Qiao, P. (2011), "Vibration-based damage identification methods: a review and comparative study", *Struct. Health Monitor.*, **10**(1), 83-111. https://doi.org/10.1177/1475921710365419

Ghiasi, R., Ghasemi, M.R. and Chan, T.H. (2021), "Optimum feature selection for SHM of benchmark structures using efficient AI mechanism", *Smart Struct. Syst., Int. J.*, **27**(4), 623-640. https://doi.org/10.12989/sss.2021.27.4.623

Giraldo, D.F., Song, W., Dyke, S.J. and Caicedo, J.M. (2009), "Modal identification through ambient vibration: comparative study", *J. Eng. Mech.*, **135**(8), 759-770. https://doi.org/10.1061/(ASCE)0733-9399(2009)135:8(759)

Goyal, D. and Pabla, B.S. (2016), "The vibration monitoring methods and signal processing techniques for structural health monitoring: a review", *Arch. Computat. Methods Eng.*, **23**(4), 585-594. https://doi.org/10.1007/s11831-015-9145-0

He, C., Li, H. and Zhao, X. (2018), "Weak characteristic determination for blade crack of centrifugal compressors based on underdetermined blind source separation", *Measurement*, **128**, 545-557. https://doi.org/10.1016/j.measurement.2018.06.047

Hyvärinen, A. and Oja, E. (2000), "Independent component analysis: algorithms and applications", *Neural Networks*, **13**(4-5), 411-430. https://doi.org/10.1016/S0893-6080(00)00026-5

Kay, S.M. (1984), "Accurate frequency estimation at low signal-to-noise ratio", *IEEE Transact. Acoust. Speech Signal Process.*, **32**(3), 540-547. https://doi.org/10.1109/TASSP.1984.1164358

Kerschen, G., Poncelet, F. and Golinval, J.C. (2007), "Physical interpretation of independent component analysis in structural dynamics", *Mech. Syst. Signal Process.*, **21**(4), 1561-1575. https://doi.org/10.1016/j.ymssp.2006.07.009

Ko, J.M. and Ni, Y.Q. (2005), "Technology developments in structural health monitoring of large-scale bridges", *Eng. Struct.*, **27**(12), 1715-1725. https://doi.org/10.1016/j.engstruct.2005.02.021

Li, H. and Ou, J. (2016), "The state of the art in structural health monitoring of cable-stayed bridges", *J. Civil Struct. Health Monitor.*, **6**(1), 43-67. https://doi.org/10.1007/s13349-015-0115-x

Li, H.N., Ren, L., Jia, Z.G., Yi, T.H. and Li, D.S. (2016), "State-of-the-art in structural health monitoring of large and complex civil infrastructures", *J. Civil Struct. Health Monitor.*, **6**(1), 3-16. https://doi.org/10.1007/s13349-015-0108-9

Li, G., Tang, G., Wang, H. and Wang, Y. (2019), "Blind source separation of composite bearing vibration signals with low-rank and sparse decomposition", *Measurement*, **145**, 323-334. https://doi.org/10.1016/j.measurement.2019.05.099

McNeill, S.I. and Zimmerman, D.C. (2008), "A framework for blind modal identification using joint approximate diagonalization", *Mech. Syst. Signal Process.*, **22**(7), 1526-1548. https://doi.org/10.1016/j.ymssp.2008.01.010

Moughty, J.J. and Casas, J.R. (2017), "A state of the art review of modal-based damage detection in bridges: development, challenges, and solutions", *Appl. Sci.*, 7(5), 510. https://doi.org/10.3390/app7050510

Musafere, F., Sadhu, A. and Liu, K. (2016), "Towards damage detection using blind source separation integrated with time-varying auto-regressive modeling", *Smart Mater. Struct.*, **25**(1), 015013. https://doi.org/10.1088/0964-1726/25/1/015013

Nagarajaiah, S. and Yang, Y. (2015), "Blind modal identification of output-only non-proportionally-damped structures by time-frequency complex independent component analysis", *Smart Struct. Syst., Int. J.*, **15**(1), 81-97. http://dx.doi.org/10.12989/.2015.15.1.081

Overschee, P.V. and Moor, B.D. (1996), *Subspace Identification for Linear Systems: Theory Implementation Application*, Kluwer Academic Publishers, Netherlands.

Parra, L. and Sajda, P. (2003), "Blind source separation via generalized eigenvalue decomposition", *J. Mach. Learn. Res.*, **4**, 1261-1269. https://doi.org/10.1162/jmlr.2003.4.7-8.1261

Peeters, B. and De Roeck, G. (2001), "Stochastic system identification for operational modal analysis: a review", *J. Dyn. Syst. Measure. Control*, **123**(4), 659-667. https://doi.org/10.1115/1.1410370

Prajapat, K. and Ray-Chaudhuri, S. (2018), "Detection of multiple damages employing best achievable eigenvectors under Bayesian inference", *J. Sound Vib.*, **422**, 237-263. https://doi.org/10.1016/j.jsv.2018.02.012

Rainieri, C., Magalhaes, F., Gargaro, D., Fabbrocino, G. and Cunha, A. (2019), "Predicting the variability of natural frequencies and its causes by Second-Order Blind Identification", *Struct. Health Monitor.*, **18**(2), 486-507. https://doi.org/10.1177/1475921718758629

Sadhu, A. and Narasimhan, S. (2014), "A decentralized blind source separation algorithm for ambient modal identification in the presence of narrowband disturbances", *Struct. Control Health Monitor.*, **21**(3), 282-302. https://doi.org/10.1002/stc.1558

Sadhu, A., Narasimhan, S. and Antoni, J. (2017), "A review of output-only structural mode identification literature employing blind source separation methods", *Mech. Syst. Signal Process.*, **94**, 415-431. https://doi.org/10.1016/j.ymssp.2017.03.001

Seo, J., Hu, J.W. and Lee, J. (2016), "Summary review of structural health monitoring applications for highway bridges", *J. Perform. Constr. Facil.*, **30**(4), 04015072. https://doi.org/10.1061/(ASCE)CF.1943-5509.0000824

Sohn, H. and Law, K.H. (1997), "A Bayesian probabilistic approach for structure damage detection", *Earthq. Eng. Struct. Dyn.*, **26**(12), 1259-1281. https://doi.org/10.1002/(SICI)1096-9845(199712)26:12<1259::AID-EQE709>3.0.CO;2-3

Spencer, B.F., Ruiz-Sandoval, M.E. and Kurata, N. (2004), "Smart sensing technology: opportunities and challenges", *Struct. Control Health Monitor.*, **11**(4), 349-368. https://doi.org/10.1002/stc.48

Tong, L., Soon, V.C., Huang, Y.F. and Liu, R. (1990), "AMUSE: a new blind identification algorithm", *Proceeding of IEEE International Symposium on Circuits and Systems*, New Orleans, LA, USA.

Vanik, M.W., Beck, J.L. and Au, S.K. (2000), "Bayesian probabilistic approach to structural health monitoring", *J. Eng. Mech.*, **126**(7), 738-745. https://doi.org/10.1061/(ASCE)0733-9399(2000)126:7(738)

Vanlanduit, S., Parloo, E., Cauberghe, B., Guillaume, P. and Verboven, P. (2005), "A robust singular value decomposition for

damage detection under changing operating conditions and structural uncertainties", *J. Sound Vib*., **284**(3-5), 1033-1050. https://doi.org/10.1016/j.jsv.2004.07.016

Weng, J.H., Loh, C.H. and Yang, J.N. (2009), "Experimental study of damage detection by data-driven subspace identification and finite-element model updating", *J. Struct. Eng*., **135**(12), 1533-1544. https://doi.org/10.1061/(ASCE)ST.1943-541X.0000079

Wu, W.H., Jhou, J.W., Chen, C.C. and Lai, G. (2019), "A novel recursive stochastic subspace identification algorithm with its application in long-term structural health monitoring of office buildings", *Smart Struct*. *Syst*., *Int*. *J*., **24**(4), 459-474. https://doi.org/10.12989/sss.2019.24.4.459

Yang, Y.B. and Chen, W.F. (2016), "Extraction of bridge frequencies from a moving test vehicle by stochastic subspace identification", *J. Bridge Eng*., **21**(3), 04015053. https://doi.org/10.1061/(ASCE)BE.1943-5592.0000792

Yang, Y. and Nagarajaiah, S. (2014), "Blind identification of damage in time-varying systems using independent component analysis with wavelet transform", *Mech*. *Syst*. *Signal Process*., **47**(1-2), 3-20. https://doi.org/10.1016/j.ymssp.2012.08.029

Yeredor, A. (2000), "Blind separation of Gaussian sources via second-order statistics with asymptotically optimal weighting", *IEEE Signal Process*. *Lett*., 7(7), 197-200. https://doi.org/10.1109/97.847367

Ying, Z.G., Ni, Y.Q. and Kang, L. (2019), "Mode localization characteristics of damaged quasiperiodically supported beam structures with local weak coupling", *Struct. Control Health Monitor*., **26**(6), e2351. https://doi.org/10.1002/stc.2351

Zhang, F.L., Ni, Y.Q., Ni, Y.C. and Wang, Y.W. (2016), "Operational modal analysis of Canton Tower by a fast frequency domain Bayesian method", *Smart Struct*. *Syst*., *Int*. *J*., **17**(2), 209-230. http://dx.doi.org/10.12989/sss.2016.17.2.209

HJ